Solutions for diffuse optical tomography using the Feynman-Kac formula and interacting particle method

Nannan Cao, Mathias Ortner, and Arye Nehorai

Department of Electrical and Systems Engineering, Washington University in St. Louis, Bryan Hall 201, Campus Box 1127, One Brookings Drive, MO, USA 63130

ABSTRACT

In this paper, we propose a novel method to solve the forward and inverse problems in diffuse optical tomography. Our forward solution is based on the diffusion approximation equation and is constructed using the Feynman-Kac formula with an interacting particle method. It can be implemented using Monte-Carlo (MC) method and thus provides great flexibility in modeling complex geometries. But different from conventional MC approaches, it uses excursions of the photons' random walks and produces a transfer kernel so that only one round of MC-based forward simulation (using an arbitrarily known optical distribution) is required in order to get observations associated with different optical distributions. Based on these properties, we develop a perturbation-based method to solve the inverse problem in a discretized parameter space. We validate our methods using simulated 2D examples. We compare our forward solutions with those obtained using the finite element method and find good consistency. We solve the inverse problem using the maximum likelihood method with a greedy optimization approach. Numerical results show that if we start from multiple initial points in a constrained searching space, our method can locate the abnormality correctly.

Keywords: Diffuse optical tomography, diffusion approximation, Feynman-Kac formula, interacting particle method, Robin boundary condition, greedy optimization method

1. INTRODUCTION

Diffuse optical tomography (DOT) is a non-invasive imaging modality that is drawing significant attention. It provides comparatively high-speed data acquisition; the instrument is portable, low-cost, and non-ionizing; and most importantly, it offers unique physiological information about hemoglobin oxygenation, which cannot be obtained through other imaging modalities. Currently, DOT is being used in areas such as functional brain imaging,[1,2] optical mammography,[3,4] as well as stroke and head trauma imaging.[5,6]

The forward model in DOT describes the photon propagation in tissue and sets up the relationship between the optical measurements and tissue's optical properties (e.g., the absorption coefficient μ_{a} and the scattering coefficient μ_{s}). It is given by the Boltzmann transport equation (TE), which can be approximated using the diffusion approximation (DA) equation under certain assumptions. Different approaches, such as the Monte Carlo (MC) method,[7,8] random walk method,[9,10] finite element method (FEM),[11,12] and finite difference method (FDM),[13,14] have been proposed to solve the forward problem. The inverse problem is to reconstruct the spatially varying μ_{a} and μ_{s} from the measurements. It is typically ill-posed and requires regularization[15] or incorporation of the prior information.[16,17]

In this paper, we propose a novel method to solve the forward problem based on DA and then provide the inverse solution. For simplicity, we assume that the tissue's scattering coefficient is known and spatially constant, and focus on reconstructing the absorption coefficient only. Our forward solution is based on the Feynman-Kac formula and interacting particle method. The Feynman-Kac formula offers a method of solving certain partial differential equations (PDEs) by simulating random paths of a stochastic process. It has been applied to areas such as mathematical finance[18,19] and stochastic physics,[20] and we used it in Ref. 21 and Ref. 22 to localize

Further author information: (Send correspondence to Arye Nehorai)
Nannan Cao: E-mail: ncao4@ese.wustl.edu, Telephone: 1 314 935 4146
Mathias Ortner: E-mail: mathias.ortner@gmail.com , Telephone: 1 314 935 4146
Arye Nehorai: E-mail: nehorai@ese.wustl.edu, Telephone: 1 314 935 7520

chemical sources under a biochemical diffusion scenario. The formula expresses the solution as an *expectation* of a *functional* of diffusion processes, which in the case of DOT is with respect to the photons' initial intensities and their spatial distributions at a certain time instance.

The forward solution can be approximated using the Monte Carlo method by simulating the photons' random walks in the medium, thereby it provides great flexibility in modeling arbitrary complex geometries and parameter distributions. The main difference from conventional MC approaches, however, is that the Feynman-Kac formula requires simulating the photons' random walks starting from the detectors and selecting only the trajectories hitting the light sources. Since the probability of such an event happening is very low, it would take a long time to get a meaningful quantity of such trajectories. To tackle this problem, we employ a multilevel Feynman-Kac method following Del Moral's work in Ref. 23. This method is based on an interacting particle approach, which reformulates the forward solution using *excursions* of photons' random walks instead of just their natural evolutions. The main reason of doing so is to select and duplicate in a dynamic way those better-fitting photons that are more likely to end in the light sources, thus are more favorable for the forward calculation.

This interacting particle method also offers the forward solver the following property: it produces a transfer kernel that is readily adaptable to computing the forward solutions associated with any μ_{a} distribution. More specifically, in order to find the best fitting μ_{a} to a certain set of measurements, it is sufficient to (i) run the MC simulation only once using an arbitrarily known absorption distribution, and (ii) keep changing μ_{a} in space and just *recompute* the forward solution associated with each one of them until the calculated observations are very close to the real measurements according to some objective functions. The computation in the second step would need the information obtained in the first step (e.g., the photon genealogical paths); however, it is very important to note that no additional MC simulations are required in this searching procedure for each possible μ_{a}.

The above method is clearly different from the conventional MC-based inverse approaches, where one needs to run a round of MC simulation for each possible μ_{a} distribution in order to find the best fitting one. As a consequence, our method can reduce the computational cost of solving the inverse problem. In the current work, we formulate the inverse solution using a perturbation-based method in a discretized parameter space.

We validate our methods using simulated 2D examples, assuming both remission and transmission geometries. In the simulation, we approximate the photon migration using a modified Euler scheme proposed by Costantini et al. in Ref. 24. We first compare the forward solution with those obtained using the FEM and find good consistency. We then solve the inverse problem using the maximum likelihood method with a greedy optimization algorithm. Numerical results show that if we start from multiple initial points in a constrained searching space, our method can locate the abnormality correctly. Our framework can be easily extended to various inverse processing approaches such as Tikhonov regularization, Bayesian estimation, or Markov random field modeling. It also allows for different optimization techniques such as simulated annealing.

This paper is organized as follows. In Section 2, we introduce our forward solution based on the DA equation and multilevel Feynman-Kac formula. In Section 3, we describe the perturbation-based inverse solution and solve it using the ML method and greedy algorithm. We then give numerical examples in Section 4 and conclude the paper in Section 5.

2. FORWARD SOLUTION USING THE MULTILEVEL FEYNMAN-KAC FORMULA

In this section, we describe our forward solution using the multilevel Feynman-Kac formula. We first briefly review the physical model of DOT given by the diffusion approximation (DA) equation. We then provide the solution to DA using the Feynman-Kac formula, followed by an extension to the multilevel case with the interacting particle method. Practical implementation using a modified Euler scheme is introduced in the end.

2.1. Physical Model of DOT

In DOT, the diffusion approximation (DA) of the Boltzmann transport equation is well accepted for modeling the photon propagation in tissue. Consider a domain $\mathcal{D}$ with boundary $\partial\mathcal{D}$, DA is given by a partial differential equation (PDE):

$$-\bigtriangledown\cdot\kappa(\boldsymbol{r})\bigtriangledown\phi(\boldsymbol{r},t)+\mu_{\mathrm{a}}\phi(\boldsymbol{r},t)+\frac{1}{c}\frac{\partial}{\partial t}\phi(\boldsymbol{r},t)=q_0(\boldsymbol{r},t),\quad\forall\boldsymbol{r}\in\mathcal{D},\tag{2.1}$$

where ϕ is the fluence (W/m^2), κ the diffusion coefficient (m), c the speed of light in the medium (m/s), and q_0 the source (W/m^3). The term κ is defined as $\kappa = 1/3(\mu_a + \mu_s')$ where $\mu_s' = (1-g)\mu_s$ is the reduced scattering coefficient (m^{-1}) with g representing the average of the cosine of the scattering angle. Since $\mu_a \ll \mu_s'$ for most biological tissues,[25] we assume $\kappa = 1/3\mu_s'$ in our calculations.

We consider the Robin boundary condition to incorporate the diffuse boundary reflection caused by a refractive index mismatch between $\mathcal{D}$ and its surrounding medium. It is given as

$$\phi(\boldsymbol{r}) + 2A\kappa(\boldsymbol{r})\frac{\partial\phi(\boldsymbol{r})}{\partial n} = 0, \quad \forall \boldsymbol{r} \in \partial\mathcal{D}, \tag{2.2}$$

where $\boldsymbol{n}$ denotes the unit outward normal of the boundary and $A = (1+R)/(1-R)$ with R representing the refraction index.

2.2. Diffusion approximation and Feynman-Kac Formula

DA can be solved using the Feynman-Kac formular, which establishes a relationship between PDEs and stochastic processes. It provides a method of solving certain PDEs by simulating random paths of a stochastic process, and the solution is given as the expectation of a functional. For the DA (2.1) with boundary condition (2.2), the Feynman-Kac formula states that the solution $\phi(\boldsymbol{r}_d, t)$ at a detector position $\boldsymbol{r}_d$ at time t can be expressed as

$$\phi(\boldsymbol{r}_d, t) = \mathbb{E}\left[\exp\left\{-c\int_0^t \mu_a(X_s)ds + \frac{1}{2A\kappa}\int_0^{t\wedge\tau} d\xi_s\right\} q_0(X_t)\right], \tag{2.3}$$

where X_s $(0 \le s \le t)$ denotes a stochastic process with $X_0 = \boldsymbol{r}_d$, ξ_s an increasing stochastic process called local time, τ the first time that X_s hits the boundary $\partial\mathcal{D}$, and $\mathbb{E}$ the expectation with respect to the probability distribution $\mathbb{P}(X_t)$. The processes X_s and ξ_s satisfy

$$\begin{cases} dX_s = \sqrt{2c\kappa}dW_s + n_s d\xi_s, \\ \xi_s = \int_0^s \mathbb{I}_{\partial\mathcal{D}}(X_r)d\xi_r, \end{cases} \tag{2.4}$$

where W_s denotes a standard Brownian motion and $\mathbb{I}(\cdot)$ the indicator function defined as

$$\mathbb{I}_A(x) = \begin{cases} 1 & \text{if } x \in A, \\ 0 & \text{otherwise} \end{cases} \tag{2.5}$$

Looking at Equation (2.3), we can see that the terms in the square brackets constitute a functional of X_s. They incorporate the effects of the optical properties of the medium (the first term in the exponential), the boundary condition (the second term in the exponential), and the source (the last term q_0). Note that unlike the usual concepts in the Monte Carlo methods or random walk theory, the Feynman-Kac formula requires that X_s be started from the detector position $\boldsymbol{r}_d$, and considers only those paths that reach the light source position (denoted by $\boldsymbol{r}_s$) for the solution (since $q_0(W_t) \neq 0$ only at $\boldsymbol{r}_s$). We illustrate the idea in Figure 1.

2.3. Diffusion approximation and Multilevel Feynman-Kac Formula

We extend the above concept using the multilevel Feynman-Kac formula where the domain is divided into several sublevels and (2.3) reformulated using *excursions* of a particle's random walks instead of its natural evolution. Furthermore, the photon's migration path is updated in a dynamic manner so that the better-fitting ones are duplicated and are more likely to end in the source locations. There are two advantages of this extension: (i) it favors the forward computation, and (ii) it produces a transfer kernel that will facilitate the inverse solution.

The multilevel Feynman-Kac formula is described in detail by Del Moral,[23] where the author provides a unified treatment on Feynman-Kac and interacting particle methods. The procedure can be outlined as follows:

(1) Domain decomposition

Let $\mathcal{D}_0 = \{\boldsymbol{r}_d\}$ denote the positions of all the detectors, $\mathcal{B}$ the source positions, and $\mathcal{A} = \partial\mathcal{D} - \mathcal{B}$. We decompose $\mathcal{D} \cup \mathcal{B}$ into a decreasing sequence of sets $\mathcal{B}_0, \mathcal{B}_1, \ldots, \mathcal{B}_m$:

$$\mathcal{B}_m \subset \mathcal{B}_{m-1} \subset \cdots \subset \mathcal{B}_1 \subset \mathcal{B}_0, \tag{2.6}$$

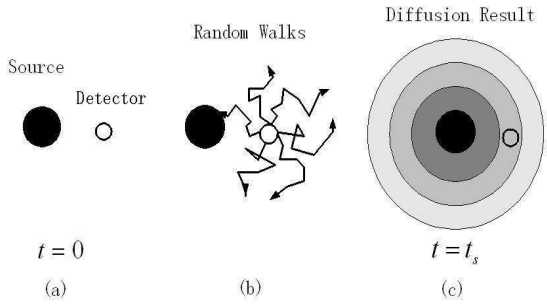

Figure 1. Illustration of solving the diffusion equation using the Feynman-Kac formula. (a) The initial condition at $t = 0$ where the disk represents a source with unit intensity ($q_0 = 1$) and the circle denotes the detector. (b) A series of stochastic processes X_s are launched from the detector to obtain the probability distribution $\mathbb{P}(X_s)$. (c) The diffusion result at $t = t_s$ computed using Equation (2.3).

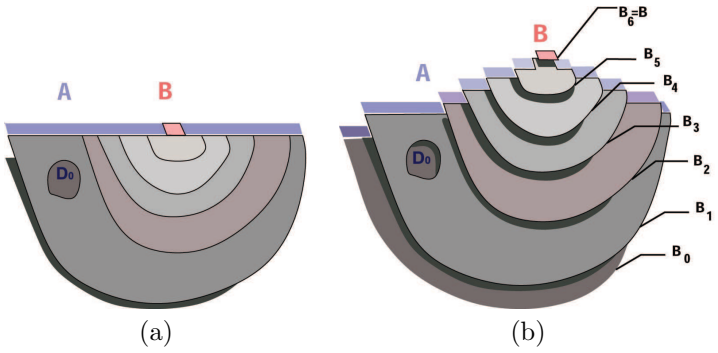

Figure 2. Illustration of the domain decomposition. In (a), $\mathcal{D}$ represents the whole domain under consideration, the detector is in $\mathcal{D}_0$, and $\mathcal{B}$ represents the source position. In (b), we decompose $\mathcal{D} \cup \mathcal{B}$ into $m = 6$ subsets such that $\mathcal{B} = B_6 \subset \mathcal{B}_5 \subset \mathcal{B}_4 \subset \ldots \subset \mathcal{B}_0$ and $\mathcal{D}_0 = \mathcal{B}_0 - \mathcal{B}_1$.

and require that $\mathcal{D}_0 = \mathcal{B}_0 - \mathcal{B}_1$ and $\mathcal{B}_m = \mathcal{B}$. See Figure 2 for an illustration. Using this setup and considering a process X_s starting from $\mathcal{D}_0$, we define the hitting time for the nth sublevel:

$$T_n = \inf\{s \geq 0 : X_s \in \mathcal{B}_n \cup \mathcal{A}\}, \qquad 1 \leq n \leq m, \tag{2.7}$$

which is the first time that X_s hits either $\mathcal{B}_n$ or $\mathcal{A}$. Note that since the sequence of sets $\mathcal{B}_n$ is increasing, we have $T_0 = 0 \leq T_1 \leq T_2 \leq \cdots \leq T_m = T$, where T is called a *stopping time*, representing the time that X_s hits the boundary $\partial\mathcal{D}$. If X_s exits $\mathcal{D}$ through $\mathcal{A}$ at some time T_k with $k < m$, we define $T_k = T_{k+1} = \cdots = T_m = T$ and say that X_s is *frozen*.

(2) Excursions and Markov Chain formulation

We define *excursions* of the process X_s as the sequence:

$$\chi_n = (T_n, (X_s)_{T_{n-1} \leq s \leq T_n}) \quad \text{with} \quad n = 1, \ldots, m \quad \text{and} \quad \chi_0 = (0, X_0), \tag{2.8}$$

which represents the evolution of X_s between successive hitting times. For a frozen process with $T = T_k$ and $k < m$, we have $\chi_{k+1} = \ldots = \chi_m = (T, X_T)$. It can be shown that the sequence $\chi_0, \chi_1, \ldots, \chi_n$ forms a Markov chain, which we will use in the later derivation. This observation is **not** obvious, coming from a strong Markov property and some conditions on the hitting times.[23]

We then define a *potential function* $\mathcal{G}_n$ for χ_n. The potential function is an important concept in our method. It captures the behavior of the particle's migration in each sublevel, which is affected by the medium properties and different boundary conditions; it also represents a "killing or creation" rate related to the absorbing nature

of the medium. For the DA equation with Robin boundary condition,

$$\mathcal{G}_n(\chi_n) = \mathbb{I}_{\mathcal{B}_n}(X_{T_n}) \exp\left\{ -c \int_{T_{n-1}}^{T_n} \mu_{\mathrm{a}}(X_s) ds + \frac{1}{2A\kappa} \int_{T_{n-1}}^{T_n} d\xi_r \right\}. \tag{2.9}$$

Clearly, for a given μ_{a}, the shorter the path the particle takes to reach $\mathcal{B}_n$, the smaller the potential. If the particle reaches the boundary $\mathcal{A}$ during the migration, its potential is 0.

Based on this definition, the forward solution (2.3) can be expressed as

$$\phi(\boldsymbol{r}_{\mathrm{d}}, t) = \mathbb{E}\left[q_0(\chi_m) \prod_{p=1}^{m} \mathcal{G}_p(\chi_p) \right]. \tag{2.10}$$

Equation (2.10) is important for the derivation of the final forward solution. It gives us a new approach to implement Monte Carlo approximations by simulating the excursions $\chi_0, \ldots, \chi_m$ of the random process X_s. Moreover, it allows the development of our novel particle updating scheme (described next), which favors the solution of the inverse problem.

(3) Interacting particle updating scheme

The particle updating scheme modifies the paths of particles in each sublevel according to their potential values. The goal is to get an unbiased expression of (2.10) while duplicating the better-fitted particles and moving them forward to explore the whole domain. By recording the genealogical histories of each particle, the inverse problem can also be solved in a simplified way.

We consider N realizations of χ_n denoted as $\varphi_n = (\varphi_n^1, \ldots, \varphi_n^i, \ldots, \varphi_n^N)$, where each φ_n^i is generated using the same Markov kernel as χ_n and is associated with a potential function $\mathcal{G}_n^i$ defined as in (2.9). We use the following two-step updating scheme:

(i) **Evolution:** A total of N photons are evolved from $t = T_n$, producing a set of φ_n.

(ii) **Selection:** A new set of photons $\hat{\varphi}_n$ are selected according to their potential values $G_n^i = \mathcal{G}(\varphi_n^i)$, since the smaller G_n^i is, the less the particle χ_n^i contributes to the forward solution. We use the following selection scheme:

$$S_n(\hat{\varphi}_n^i, \cdot) = \frac{G_n^i}{\max\{G_n^j\}} \delta_{\varphi_n^i}(\cdot) + (1 - \frac{G_n^i}{\max\{G_n^j\}}) \Psi_n^N(\cdot), \tag{2.11}$$

where the first term on the right represents the probability of χ_n^i staying, and the second term is the probability of it being replaced. More specifically,

- with a probability $\frac{G_n^i}{\max\{G_n^j\}}$, the particle stays where it is, i.e., $\hat{\varphi}_n^i = \varphi_n^i$;
- otherwise, it is replaced by a new $\hat{\varphi}_n^i$, which is randomly selected according to the distribution

$$\Psi_n^N(\cdot) = \frac{1}{\sum_{j=1}^N G_n^j} \sum_{j=1}^N G_n^j \delta_{\varphi_n^j}(\cdot). \tag{2.12}$$

We illustrate the above procedure in Figure 3. We can see that this algorithm is built such that:

- If a particle reaches $\mathcal{A}$, it will always be discarded and replaced by a "better" one which hits $\mathcal{B}_i$. A direct consequence of this scheme is that each photon will evolve in a direction "more favorable" to our calculation.
- There are always N trajectories evolving in the medium, and we will obtain N photons in $\mathcal{B}$ in the end.

As a consequence, Equation (2.10) is approximated using results of Ref. 23 as

$$\phi(\boldsymbol{r}_{\mathrm{d}}, t) = \frac{1}{N^m} \prod_{p=0}^{m-1} \left[\sum_{j=1}^N G_p^j \right] \times \sum_{j=1}^N G_m^j q_0(\varphi_m^j). \tag{2.13}$$

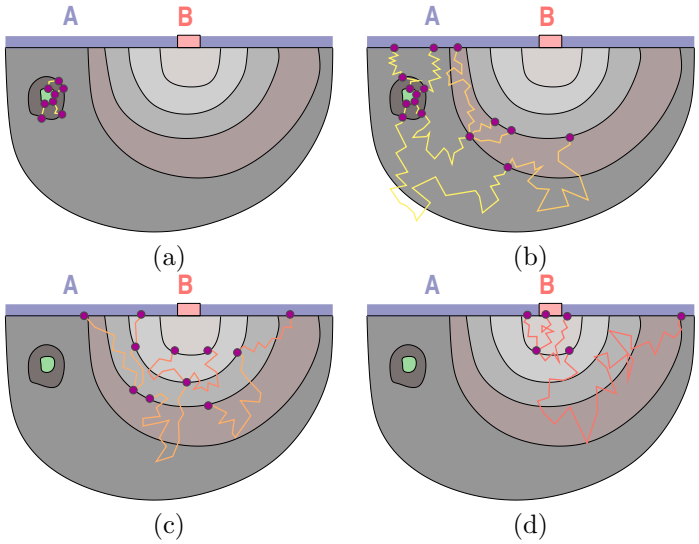

Figure 3. Illustration of successive steps of photon migrations using the multilevel Feynman-Kac formula. In this case, $m = 6$ levels and $N = 4$ photons. (a) The photons are launched from the set $\mathcal{D}_0$ and all reach $\mathcal{B}_0$. (b)-(d) The photons progress through the domain. At each level, the trajectories hitting the "bad set" $\mathcal{A}$ of the boundary are stopped and replaced by the good trajectories selected randomly according to Equation (2.12). In the end, all four photons end up in the subset $\mathcal{B} = \mathcal{B}_6$ and contribute to the observation.

2.4. Implementation of the Forward Solution

In order to implement the forward solution (2.13) using the Monte Carlo method, we need to find a scheme to simulate the photon migration (i.e., Equation (2.4)) in a discrete manner. We use the modified Euler scheme given by Costantini (see Ref. 24 for details). Denote h the temporal discretization step and N_p the number of random walks in the p^{th} sublevel, the potential function is approximated as

$$\mathcal{G}_p^i(t, X) = \mathbb{I}_{\mathcal{B}_n}(X_t) \exp\left\{-ch \sum_{l=1}^{N_p} \mu_{\mathrm{a}}(X_l) + \frac{h}{2A\kappa} \sum_{l=1}^{N_p} \xi_l\right\}, \tag{2.14}$$

and (2.13) can then be computed accordingly.

3. INVERSE SOLUTIONS

In this section, we solve the inverse problem using a perturbation-based method in a discretized parameter space. We compute it using the maximum likelihood method with a greedy optimization algorithm.

3.1. Perturbation-based Inverse Solution

The inverse problem in DOT is to estimate $\mu_{\mathrm{a}}(\boldsymbol{r})$ from ϕ. It does not look easy from (2.13), since μ_{a} exists only in G and its relationship to ϕ is highly nonlinear. To tackle this issue, we propose a perturbation-based algorithm. The key idea is that if we assume a known μ_{a} and run MC simulations using the multilevel Feynman-Kac formula, saving each particle's potential value G on each sublevel along with its genealogical history, then the observation $\bar{\phi}$ associated with any other $\bar{\mu}_{\mathrm{a}}$ can be *computed* directly using the saved information without running additional MC simulations. The feasibility of this method is based on the following result:[23]

$$\bar{\phi}(\boldsymbol{r}_{\mathrm{d}}, t) = \frac{1}{N^m} \prod_{p=0}^{m-1} \Big(\sum_{j=1}^{N} G_p^j\Big) \times \sum_{j=1}^{N} \left(G_m^j \times \prod_{p=0}^{m} \frac{\bar{\mathcal{G}}_p(\mathrm{Anc}(\varphi_m^j, p))}{\mathcal{G}_p(\mathrm{Anc}(\varphi_m^j, p))} q_0(\xi_m^j) \right), \tag{3.15}$$

where $\mathrm{Anc}(\varphi_m^j, p)$ represents the ancestor of the particle φ_m^j at level p, G_p^j the potential value of φ_p^j at level p, $\mathcal{G}_p$ the potential function defined in (2.9) for the known μ_{a}, and $\bar{\mathcal{G}}$ same as in (2.9) but for the unknown $\bar{\mu}_{\mathrm{a}}$.

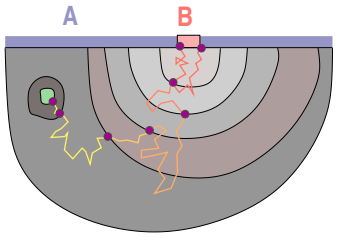

Figure 4. An example of the ancestors of two photons.

Among all these four quantities, the first three are associated with μ_{a} and are known *a priori*. The only factor that is affected by $\bar{\mu}_{\mathrm{a}}$ is $\bar{\mathcal{G}}$, which, however, is also calculated using the genealogical histories obtained from μ_{a}. In Figure 4 we give an example of the genealogical tree of two photons at level m, composed of their ancestors.

Therefore, according to Equation (3.15), we can find the inverse solution $\hat{\mu}_{\mathrm{a}}$ by continuing to change $\bar{\mu}_{\mathrm{a}}$ (recomputing only one term ($\bar{\mathcal{G}}$) each time) until a calculated $\bar{\phi}^s$ is as close as possible to the real measurements according to some objective functions. We claim that $\hat{\mu}_{\mathrm{a}} = \bar{\mu}_{\mathrm{a}}^s$.

This procedure reduces the computations compared with the conventional Monte Carlo method. The MC method requires *rerunning* a complete simulation of the particle's evolution for a different $\bar{\mu}_{\mathrm{a}}$, which is computationally very expensive. After substituting (2.14) into (3.15), we can easily obtain

$$\bar{\phi} = \frac{1}{N^m} \prod_{p=0}^{m-1} (\sum_{j=1}^{N} G_p^j) \times \sum_{j=1}^{N} \left(G_m^j \times \exp\left\{ -ch \sum_{p=0}^{m} \sum_{l=1}^{N_p} \delta\mu_{\mathrm{a}}(\mathrm{Anc}(\varphi_m^j, p)) \right\} \phi_0(\xi_m^j) \right), \tag{3.16}$$

where $\delta\mu_{\mathrm{a}} = \bar{\mu}_a - \mu_{\mathrm{a}}$. We can see that the last term in (2.14) related to the local time is canceled out and does not contribute to the final solution. This observation actually simplifies the computation, since we do not need to save the information of ξ during the simulation with μ_{a}.

Actually, as we will show later, calculating $\bar{\mathcal{G}}$ can be further simplified after we discretize the function μ_{a} in space. We will show that we need to consider only the *spatial difference* between the discretized μ_{a} and $\bar{\mu}_{\mathrm{a}}$ in order to obtain $\bar{\phi}$.

3.2. Domain Discretization

In order to estimate the spatial distribution of μ_{a}, we discretize the domain $\mathcal{D}$ into N_{a} small elements $\mathcal{D}_i$ such that

$$\mathcal{D} = \bigcup_{i=1}^{N_{\mathrm{a}}} \mathcal{D}_i \quad \text{and} \quad \mathcal{D}_i \cap \mathcal{D}_j = \emptyset, \ \forall i \neq j. \tag{3.17}$$

We assume constant $\mu_{\mathrm{a}i}$ in each element and express the spatial distribution of μ_{a} as $\mu_{\mathrm{a}} = \sum_{i=1}^{N_{\mathrm{a}}} \mathbb{I}_{\mathcal{D}_i} \mu_{\mathrm{a}i}$. In this way, the inverse solution is estimating $\{\mu_{\mathrm{a}i}\}$ from the measurements.

This discretization step has the following effect on computing (3.16): when we record $\mathrm{Anc}(\cdot)$ for each sublevel, instead of saving the exact position of the photon along each path, now we only need to record how many times the photon passes element $\mathcal{D}_i$ in each sublevel. Denote this number by $N_{i,p}$. Then (3.16) becomes

$$\bar{\phi} = \frac{1}{N^m} \prod_{p=0}^{m-1} (\sum_{j=1}^{N} G_p^j) \times \sum_{j=1}^{N} \left(G_m^j \times \exp\left\{ -ch \sum_{i=1}^{N_{\mathrm{a}}} N_{i,p} \delta\mu_{\mathrm{a}i} \right\} q_0(\xi_m^j) \right), \tag{3.18}$$

which is the formula we will use for the inverse solution.

3.3. Maximum Likelihood Method

We propose to solve the inverse problem using the maximum likelihood method. We assume a zero-mean additive Gaussian noise $\boldsymbol{e}$ that is spatially uncorrelated with an unknown variance σ_e^2, i.e., $\boldsymbol{e} \sim \mathcal{N}(0, \sigma_e^2 I)$. We formulate the measurement model as

$$\boldsymbol{y} = \boldsymbol{g}(\boldsymbol{\mu_a}, \boldsymbol{f}) + \boldsymbol{e}, \tag{3.19}$$

where $\boldsymbol{y} = [y_1, y_2, \ldots, y_{N_\mathrm{d}}]^T$ is the measurement vector, $\boldsymbol{e} = [e_1, e_2, \ldots, e_{N_\mathrm{d}}]^T$ the noise vector, and $\boldsymbol{g} = [g_1, g_2, \ldots, g_{N_\mathrm{d}}]^T$ with each g_i given in (3.18). The term $\boldsymbol{f} = \{f_1, f_2, \ldots, f_{N_\mathrm{s}}\}$ represents the known source intensities and $\boldsymbol{\mu_a} = \{\mu_{\mathrm{a}1}, \mu_{\mathrm{a}2}, \ldots, \mu_{\mathrm{a}N_\mathrm{a}}\}$ the discretized absorption coefficient in each element. In order to find the optimal $\boldsymbol{\mu_a}$ for the given $\boldsymbol{y}$, we need to minimize the following objective function:

$$J(\boldsymbol{\mu_a}) = ||\boldsymbol{y} - \boldsymbol{g}||^2. \tag{3.20}$$

3.4. Greedy Algorithm

It is clear that the above inverse problem is highly nonlinear with respect to the unknown $\boldsymbol{\mu_a}$. It is also underdetermined because of the large number of unknowns (μ_{a_i}'s) and limited number of measurements. We propose to estimate $\boldsymbol{\mu_a}$ using the greedy optimization algorithm (GOA). GOA is a numerical method that selects a locally optimum choice at each stage with the hope of finding the global optimum. For simplicity, we assume that there is only one abnormality in the domain. We denote the normal μ_a as μ_a^1 and the abnormal one as μ_a^2, and thus the elements in $\boldsymbol{\mu_a}$ are composed of $\{\mu_\mathrm{a}^1, \mu_\mathrm{a}^2\}$. The procedure of GOA is described as follows.

- Start from an arbitrary μ_a distribution and discretize it in space, obtaining a $\boldsymbol{\mu_{a0}}$.
- Generate a random number ind uniformly distributed in $[1, N_\mathrm{a}]$ and flip the ind^{th} element in $\boldsymbol{\mu_{a0}}$, i.e., if $\mu_{\mathrm{a}_\mathrm{ind}} = \mu_\mathrm{a}^1$, let $\mu_{\mathrm{a}_\mathrm{ind}} = \mu_\mathrm{a}^2$; otherwise, $\mu_{\mathrm{a}_\mathrm{ind}} = \mu_\mathrm{a}^1$. Name the flipped μ_a distribution $\boldsymbol{\mu_{a1}}$.
- Compute (3.20) using $\boldsymbol{\mu_{a0}}$ and $\boldsymbol{\mu_{a1}}$. If $J(\boldsymbol{\mu_{a1}}) < J(\boldsymbol{\mu_{a0}})$, accept the change; otherwise, keep $\boldsymbol{\mu_{a0}}$.
- Repeat the computation until the minimum value is reached or the number of iterations exceeds a prescribed value N_maxiter.

For most problems, GOA is not guaranteed to converge to the globally optimal solution, since it usually does not operate exhaustively on all the data. To avoid this problem, we implement GOA using different initial points to find the best fitting μ_a. Additionally, we constrain our searching space according to our foreknowledge, in order to ameliorate the underdetermined nature of the problem.

4. NUMERICAL EXAMPLES

In this section, we present numerical examples to (i) validate our forward solution, and (ii) illustrate the applicability of our inverse solutions.

4.1. Comparison to FEM

We first analyze the validity of our forward solution by comparing it to the FEM, which is commonly used in DOT.[11,12] We consider a 2D rectangular domain of size 8×10 cm^2. We assume two sources at $\boldsymbol{r}_{\mathrm{s}1} = (-2, 0)$ cm, $\boldsymbol{r}_{\mathrm{s}2} = (2, 0)$ cm, and three detectors at $\boldsymbol{r}_{\mathrm{d}1} = (-4, 0)$ cm, $\boldsymbol{r}_{\mathrm{d}2} = (0, 0)$ cm, and $\boldsymbol{r}_{\mathrm{d}3} = (4, 0)$ cm. We assume that each source has a unit intensity and the source fiber has a radius of 3mm.

The simulation setup is illustrated in Figure 5. In our forward simulations, we divide the space between all the source-detector pairs into six sublevels as is shown in Figure 5 using different red levels. We assume $\kappa = 0.06$ cm, $c = 22$ cm/ns, and $A = 3.24$ in the domain, which are close to the real values for biological tissue.[26]

We consider the following two cases for the validation. In the first case, we assume homogeneous absorption coefficient $\mu_\mathrm{a} = 0.2$ cm^{-1} throughout the whole domain, whereas in the second case, we assume a 2×1.5 cm^2 rectangular abnormality centered at $(1, -1.25)$ cm. The abnormality has an absorption coefficient $\mu_\mathrm{b} = 0.6$ cm^{-1}. In each case, we compute the optical fluences at three detectors using both FEM and our proposed method.

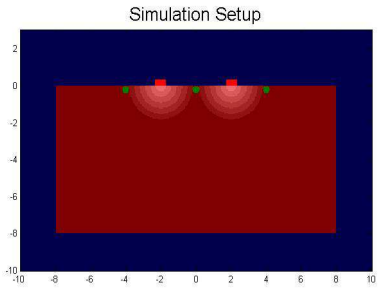

Figure 5. 2D simulation setup (in cm units). The two small rectangles represent the source light fibers with radius 3mm, the dots the detectors, and the semicircle areas with different red levels denote the sublevels we constructed for the forward calculation.

Table 1. FEM Results (in mW/cm^2) Using Different Absorption Distributions.

μ_a Distribution	ϕ_{d1}	ϕ_{d2}	ϕ_{d3}
Case 1	4.585	9.176	4.584
Case 2	4.584	6.507	4.338

The FEM solutions are given in Table 1. They were obtained using the software FEMLAB, where we divided the domain into 126,720 triangular elements and applied Lagrange quadratic polynomials as interpolation functions. Considering the fine nature of this tessellation, we claim that the values we obtained are very close to the real solutions.

We launched 10^6 photons to compute our forward solutions. The simulation was performed using Matlab 7 on a PC with Pentium 4 2.6GHz CPU and 1G of RAM. Because of the Monte Carlo nature of our method, we cannot obtain a single exact forward solution, since the observation ϕ varies with a small variance among different realizations. As a consequence, we use the function "boxplot()*" in Matlab in order to make the comparison. The boxplots (labeled as "MC") for three detectors are given in Figure 6, where the first row represents the results using homogenous μ_a distribution and the second row corresponds to the μ_a with the rectangular abnormality. In each figure, the FEM result (labeled as "FEM") is also plotted to the right of the box. We can see that the FEM solutions always fall within the range of each box (around the median of the distribution), which indicates that our method provides good approximations to the true forward solutions.

4.2. Inverse Solutions

We tested our inverse method using a transmission geometry as shown in Figure 7a. The domain is of size 6×12 cm^2, where 9 sources are placed on the top surface and 9 detectors on the bottom. A 1×2 cm^2 rectangle abnormality with $\mu_b = 0.5$ cm^{-1} is inserted with its center at (2.5,3) cm, and the the background absorption coefficient is assumed to be $\mu_a = 0.2$ cm^{-1}. We imposed additive Gaussian noises and chose the noise variance such that the signal-to-noise ratio (SNR) was 20dB. We defined the SNR as SNR $= 10\log((\sum_{i=1}^{N_d}\phi_i^2)/\sigma_e^2)$, where $\phi_i = g_i(\boldsymbol{\mu_a}, \boldsymbol{f})$ represents the calculated observation at the ith detector.

We discretized the domain into small elements of size 2.5×2.5 mm^2 and applied the greedy optimization algorithm for the inverse solutions. In our case, since we know the correct position of the abnormality, we simplify the inverse computations by (i) randomly picking an initial point within the range $x \in [0, 6]$ cm, $y \in [-1, -5]$ cm, and (ii) updating the $\boldsymbol{\mu_a}$ in the same range according to the scheme we introduced in Subsection 3.4. In

*A boxplot produces a box-and-whisker plot for a set of data, providing a good visual summary of the important aspects of a distribution. The box stretches from the lower hinge (defined as the 25th percentile) to the upper hinge (the 75th percentile) and also indicates the median as a line across the box. The whiskers are lines extending from each end of the box to show the extent of the data.

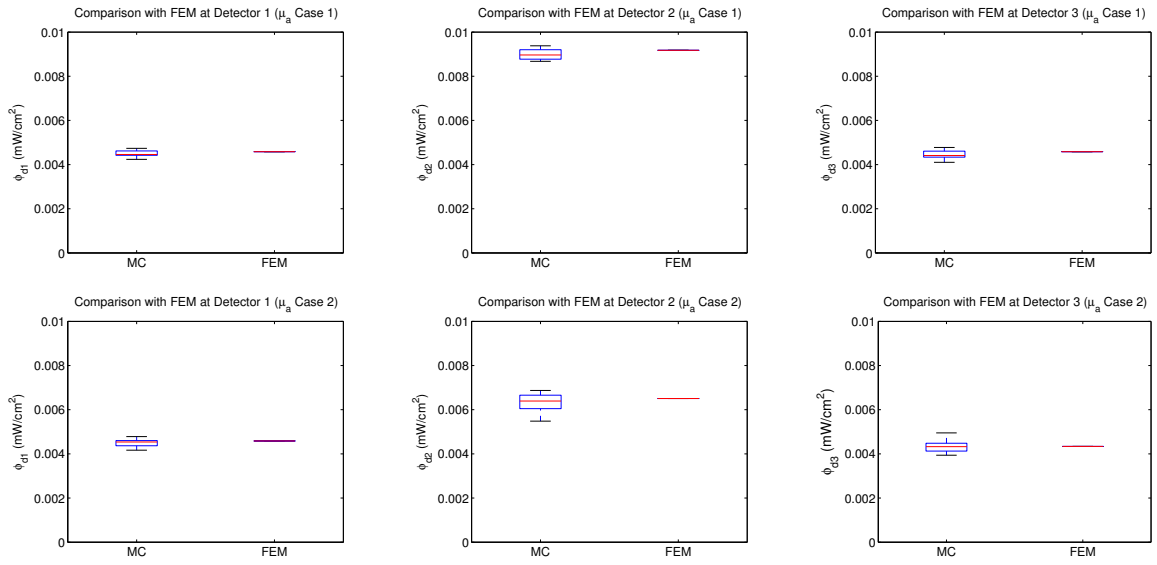

Figure 6. Box plots of the simulated forward solutions for DOT using our method compared with FEM. The first row represents results at different detectors with homogeneous μ_a distribution, and the second row is for the heterogeneous μ_a distribution with a rectangle abnormality.

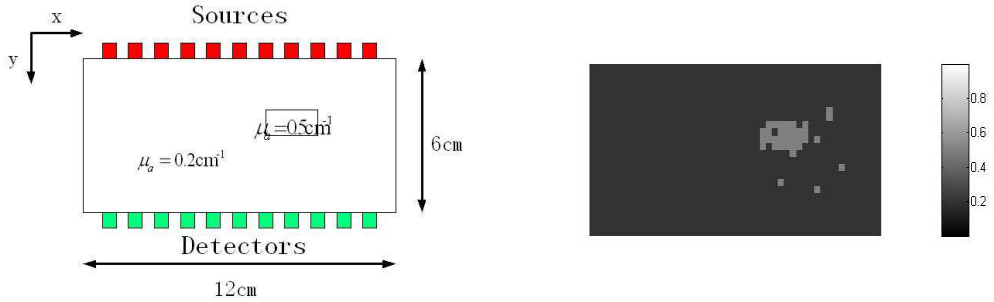

Figure 7. Estimation results of the abnormality using the greedy optimization method. (a) Simulation setup. (b) Inverse solutions of the absorption distribution.

order to avoid being stuck in the local minimum, we used different initial points and picked the μ_a configuration leading to the least objective function value as our final solution. The estimated absorption distribution is shown in Figure 7b. We can see that the abnormality was recovered at the correct location.

5. CONCLUSIONS

In this paper, we introduced the application of Feynman-Kac formula and interacting particle method to solve the forward and inverse problems in DOT. Our method is based on the diffusion approximation and belongs to the class of Monte Carlo methods. Therefore, it can be applied to arbitrary complex geometries and parameter distributions. However, unlike the conventional MC approaches, it has the following features:

- It uses excursions of the photons' random walks instead of their natural evolutions.
- It updates the photon evolution in a dynamical way (according to its potential values) such that the better-fitted photons are duplicated and moved forward.

- It requires only one round of MC simulations in order to get observations from different optical parameter distributions. This property is based on recording the photons' genealogical histories, and greatly favors the inverse computation.

We validated the proposed forward solution method by comparing it with FEM and found good consistency. We developed a maximum likelihood estimator and computed it numerically using the greedy optimization method in a constrained searching space. We found that assuming a single abnormality and starting from different initial points, our approach can localize the anomaly correctly. It is known that the greedy algorithm often suffers from the problem of being trapped in a local minimum. In this paper, we tackled this issue by using multiple initial values. An alternative method would be to apply the simulated annealing (SA) algorithm, which guarantees convergence to the global minimum.

We have applied our methods to both remission measurements, which has the potential application to brain tomography, and transmission geometries, which can be useful for breast imaging. We will extend our work to the 3D case, which is of interest in real applications. We will also consider a layered head model (e.g., the one obtained using MRI) and explore the effects of different noise models (e.g., the Poisson noise).

ACKNOWLEDGMENTS

This work was supported by the National Science Foundation Grants CCR-0330342 and CCF-0630734.

REFERENCES

1. G. Strangman, D. Boas, and J. Sutton, "Non-invasive neuroimaging using near-infrared light," *Biol. Psychiatry* **52**, pp. 679–693, 2002.
2. A. Villringer and B. Chance, "Non-invasive optical spectroscopy and imaging of human brain function," *Trends in Neuroscience* **20**, pp. 435–442, 1997.
3. D. Grosenick, T. Moesta, H. Wabnitz, J. Mucke, C. Stroszcynski, R. Macdonald, P. Schlag, and H. Rinnerberg, "Time-domain optical mammography: initial clinial results on detection and characterization of breast tumors," *Appl. Opt.* **42**, pp. 3170–3186, 2003.
4. H. Jiang, N. Iftimia, J. Eggert, L. Fajardo, and K. Klove, "Near-infrared optical imaging of the breast with model-based reconstruction," *Acad. Radiol.* **9**, pp. 186–194, 2002.
5. D. A. Benaron, S. R. Hintz, A. Villringer, D. Boas, A. Kleinschmidt, J. Frahm, C. Hirth, H. Obrig, J. C. van Houten, E. L. Kermit, W. F. Cheong, and D. K. Stevenson, "Noninvasive functional imaging of human brain using light," *J. Cereb. Blood Flow Metab.* **20**, pp. 469–477, 2000.
6. S. R. Hintz, W. F. Cheong, D. K. Stevenson, and D. A. Benaron, "Beside imaging of intracranial hemorrhage in the neonate using light: Comparison with ultrasound, computed tomography, and magnetic resonance imaging," *Pediatr. Res.* **45**, pp. 54–59, 1999.
7. D. A. Boas, J. P. Culver, J. J. Stott, and A. K. Dunn, "Three dimentional Monte Carlo code for photon migration through complex heterogeneous media including the adult human head," *Optics Express* **10**, pp. 159–170, Feb. 2002.
8. L. Wang, S. L. Jacques, and L. Zheng, "Mcml-Monte Carlo modeling of light transport in multi-layered tissues," *Computer Methods and Programs in Biomedicine* **47**, pp. 131–146, 1995.
9. A. H. Gandjbakhche, G. H. Weiss, F. R. Bonner, and R. Nossal, "Photon path-length distributions for transmission through optically turbid slabs," *Physical review E* **48**, pp. 810–818, August 1993.
10. A. H. Gandjbakhche and G. H. Weiss, "Random walk and diffusion-like models of photon migration in turbid media," *Progress in Optics* , pp. 333–401, 1995.
11. S. R. Arridge, M. Schweiger, M. Hiraoka, and D. T. Delpy, "A finite element approach for modeling photon transport in tissue," *Med. Phys.* **20**, pp. 299–309, 1993.
12. M. Schweiger, S. R. Arridge, M. Hiraoka, M. Firbank, and D. T. Deply, "Comparison of a finite element forward model with experimental phantom results: Application to image reconstruction," **1888**, pp. 179–190, 1993.

13. B. W. Pogue, M. S. Patterson, H. Jiang, and K. D. Paulsen, "Initial assessment of a simple system for frequency domain diffuse optical tomography," *Phys. Med. Biol.* **40**, pp. 1709–1729, 1995.
14. W. F. Ames, *Numerical methods for partial differential equations*, Academic, New York, 2 ed., 1977.
15. B. Pogue, T. McBride, J. Prewitt, U. Osterberg, and K. Paulsen, "Spatially variant regularization improves diffuse optical tomography," *Appl. Opt.* **38**, pp. 2950–2961, May 1999.
16. M. Guven, B. Yazici, X. Intes, and B. Chance, "Diffuse optical tomography with a priori anatomical information," *Phys. Med. Biol.* **50**, pp. 2837–2858, 2005.
17. J. C. Ye, C. A. Bouman, K. J. Webb, and R. P. Millane, "Nonlinear multigrid algorithms for bayesian optical diffuse tomography," *IEEE Trans. Image Processing* **10**, pp. 909–922, 2001.
18. D. Nualart and W. Schoutens, "Bsde's and Feynman-Kac formula for Levy processes with applications in finance," *Bernoulli* **7**, pp. 761–776, 2001.
19. J. M. Steele, *Stochastic calculus and financial applications*, Springer-Verlag, New York, 2003.
20. A. S. Sznitman, *Brownian motion obstacles and random media*, Springer-Verlag, New York, 1998.
21. M. Ortner, A. Nehorai, and A. Jeremic, "Biochemical transport modeling and bayesian source estimation in realistic environments," *IEEE Signal Process. Magazine* , 2005.
22. M. Ortner and A. Nehorai, "Biochemical transport modeling and sequential detection in realistic environments," *IEEE Signal Process. Magazine* , 2005.
23. P. Del Moral, *Feynman-Kac Formulae, "Genealogical and interacting particle systems with applications"*, Springer-Verlag, New York, 2004.
24. C. Costantini, B. Pacchiarotti, and F. Sartoretto, "Numerical approximation for functionals of reflecting diffusion processes," *SIAM J. Appl. Math.* **58**, pp. 73–102, Feb. 1998.
25. S. R. Arridge, "Optical tomography in medical imaging," *Inverse Problems* **15**, pp. R41–R93, 1999.
26. A. Y. Bluestone, M. Stewart, J. Lasker, G. S. Abdoulaev, and A. H. Hielscher, "Three dimensional optical tomographic brain imaging in small animals, part 1: Hypercapnia," *Journal of Biomedical Optics* **9**, pp. 1046–1062, 2004.